LA-UR-18-24121 (Accepted Manuscript)

Plasmonic Hot-Carrier-Mediated Tunable Photochemical Reactions

Zhang, Yu
Nelson, Tammie Renee
Tretiak, Sergei
Guo, Hua
Schatz, George C.

To be published in: ACS Nano

DOI to publisher's version: 10.1021/acsnano.8b03830

Permalink to record: http://permalink.lanl.gov/object/view?what=info:lanl-repo/lareport/LA-UR-18-24121

ACS NANO
Cite This: ACS Nano XXXX, XXX, XXX−XXX
www.acsnano.org

ARTICLE

Plasmonic Hot-Carrier-Mediated Tunable Photochemical Reactions

Yu Zhang,*[,†,‡] Tammie Nelson,[†] Sergei Tretiak,[†] Hua Guo,[§] and George C. Schatz[‡]

[†]Physics and Chemistry of Materials, Theoretical Division, Los Alamos National Laboratory, Los Alamos, New Mexico 87545, United States

[‡]Department of Chemistry, Northwestern University, 2145 Sheridan Road, Evanston, Illinois 60208, United States

[§]Department of Chemistry and Chemical Biology, University of New Mexico, Albuquerque, New Mexico 87131, United States

Supporting Information

ABSTRACT: **Hot-carrier generation from surface plasmon decay has found applications in many branches of physics, chemistry, materials science, and energy science. Recent reports demonstrated that the hot carriers generated from plasmon decay in nanoparticles can transfer to attached molecules and drive photochemistry which was thought impossible previously. In this work, we have computationally explored the atomic-scale mechanism of a plasmonic hot-carrier-mediated chemical process, H_2 dissociation. Numerical simulations demonstrate that, after photoexcitation, hot carriers transfer to the antibonding state of the H_2 molecule from the nanoparticle, resulting in a repulsive-potential-energy surface and H_2 dissociation. This process occurs when the molecule is close to a single nanoparticle. However, if the molecule is located at the center of the gap in a plasmonic dimer, dissociation is suppressed due to sequential charge transfer, which efficiently reduces occupation in the antibonding state and, in turn, reduces dissociation. An asymmetric displacement of the molecule in the gap breaks the symmetry and restores dissociation when the additional charge transfer is significantly suppressed. Thus, these models demonstrate the possibility of structurally tunable photochemistry *via* plasmonic hot carriers.**

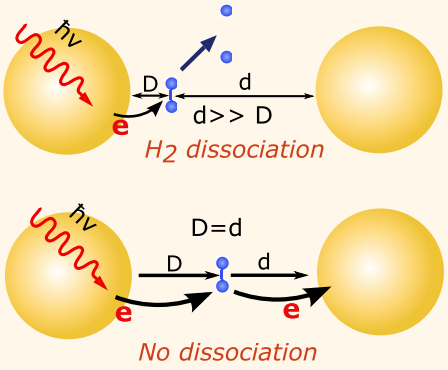

KEYWORDS: *plasmonics, charge transfer, hot carriers, photocatalysis, plasmonic energy conversion, H_2 dissociation*

Surface plasmon polaritons (SPPs) and localized surface plasmon resonances (LSPRs) are collective oscillations of electrons in conductors excited by electromagnetic modes that are confined to conductor−dielectric interfaces.[1−3] Exciting the surface plasmons results in the concentration of light in the near-field around the particle interfaces,[4,5] which enables efficient spatial control of charge, and energy fluxes in a variety of applications. However, surface plasmons suffer from significant dissipation,[6] with most of the plasmon's energy loss due to Landau damping leading to hot electron−hole (e−h) pairs. Then, the hot electrons and holes redistribute their energy, and the temperature of the conduction electrons increases due to electron−electron scattering process. Electron−phonon scattering results in further dissipation of the energy of hot carriers, raising the lattice temperature of the particle. This energy is ultimately dissipated to the environment *via* thermal conduction. Ultrafast hot-carrier generation dominates the energy dissipation of SPPs,[7] which limits plasmonics applications due to the short plasmon lifetime. Several recent efforts have proposed the possible extraction of hot carriers before dissipation takes place.[8−10] This has simulated the application of hot carriers to several branches of applied physics, chemistry, and materials and energy sciences.[11−20]

Even though our recent theoretical studies have shown that extracting hot carriers for solar energy conversion suffers from fundamental limitations,[21] the opportunities for using plasmonic hot-carrier extraction to drive photochemistry are less-well-known. Photochemical reactions enable the primary event in vision,[22] photosynthesis in plants,[23] gating of certain ion channels,[24] and other biological processes. Plasmon-driven photochemistry has received increasing attention in recent years for its potential for overcoming the intrinsic limitations of conventional semiconductor photocatalysis. Recent studies have shown that the generated hot carriers in plasmonic structures can be transferred to adjacent electron acceptors, inducing such photochemical processes as H_2, O_2, and N_2 dissociation,[25−32] water splitting,[33−37] artificial photosynthesis,[38] and hydrocarbon conversion.[39] The unique feature that the optical properties of metallic nanoparticles (NPs) are tunable over a wide range of the spectrum *via* size, shape, and

Received: May 21, 2018
Accepted: July 12, 2018
Published: July 12, 2018

DOI: 10.1021/acsnano.8b03830
ACS Nano XXXX, XXX, XXX−XXX

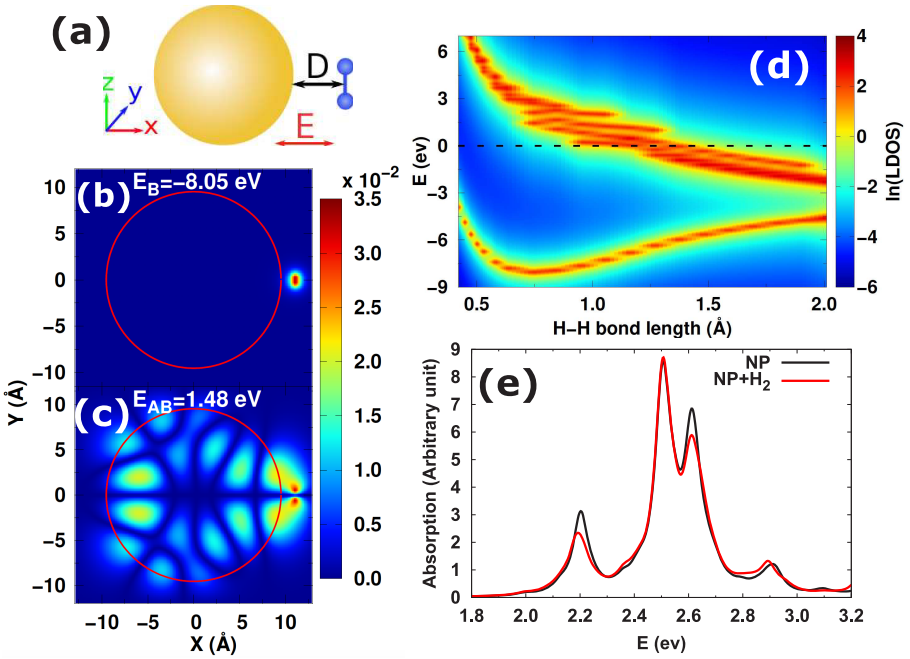

Figure 1. (a) Schematic diagram of H_2 molecule adsorbed on the NP surface. The electric field is in x direction. (b) Bonding and (c) antibonding (AB) wave functions of H_2 in the x−z plane. Panel c indicates that (1) the AB state is 1.48 eV above the Fermi energy, which offers the possibility of transferring the hot-electron generated in the metallic NPs to the AB state; and (2) the AB WF is hybridized with the NP, which can facilitate the hot-electron transfer. The red circle indicates the surface of the NP. (d) LDOS of H_2 adsorbed on NP surface. The dashed line indicates the Fermi energy (shifted to 0) of the NP + H_2 system with equilibrium H−H bond length. The evolution of peaks in LDOS for different H−H bond lengths roughly reflects the PES of the H_2 molecule. (e) Absorption spectrum of NP and NP + H_2.

composition makes the NPs an ideal candidate for plasmon-induced chemistry.[5] The NPs used in photochemistry are typically gold spheres with sizes as small as several nanometers. However, the optimal structure for plasmonic enhancement in hot-electron-mediated chemical reactions is still an open question. Hence, understanding plasmon-driven chemistry in a realistic environment is crucial for further development.

In this work, we demonstrate the principles of the plasmonic enhancement and control of chemical reactions by considering the photoinduced dissociation of an adsorbed molecule on a plasmonic nanoparticle and plasmonic dimer. *Ab initio* non-adiabatic molecular dynamics (NAMD) calculations are performed for H_2 dissociation into individual hydrogen atoms on metallic NPs after being excited by femtosecond laser pulses by employing time-domain time-dependent density functional theory (TDDFT) and Ehrenfest dynamics. Our results show that the hot-carrier transfer to the antibonding orbital of H_2 attached to a monomer nanoparticle is quite feasible and can lead to dissociation. However, for the plasmonic dimer, a competing process involves sequential transfer of the electron to H_2 and then to the other nanoparticle. This reduces dissociation, which becomes tunable depending on spatial location of the molecule in between the nanoparticles, with the minimal dissociation being associated with the most-significant electromagnetic hot spot.

RESULTS

Computational Approach. The NAMD calculations were performed with the OCTOPUS package,[40−42] with the metal NP treated in the Jellium approximation. The Jellium radius is carefully chosen so that the resonant frequencies (around 2.5 eV) are similar to that of a Au nanoparticle with a diameter of several nanometers. For feasibility, we chose the size of the metallic NP (diameter) to be 19.05 Å, corresponding roughly to a 200 atom gold cluster. While this size is smaller than in the experiments to date, the plasmonic properties of such particles are similar to those of much larger particles except for a size-dependent blue shift of the plasmon.[43] The distance between the H_2 molecule and NP is set to be 1.59 Å, which is a stable distance as confirmed by the Born−Oppenheimer molecular dynamics (BOMD) simulation. In addition, the H_2 molecule is placed parallel to the NP surface, as shown by the schematic diagram in Figure 1a. A maximum field strength of E_{max} = 2.57 V/Å is assumed for the laser pulse in the simulations. Other details of the calculations can be found in the Methods section.

Plasmonic Hot-Carrier-Induced H_2 Dissociation on the NP Surface. We start by examining the electronic structure of H_2 adsorbed on the NP, where the wave functions (WFs) of H_2 and the NP become hybridized at chemically relevant separations. Analysis of the weight (w_i) of H_2 to each WF shows that the bonding and antibonding (AB) state (the states that have the largest w_i) of the H_2 are 8.05 eV below and 1.48 eV above the Fermi energy, as shown by Figure 1b−d. Because of the gap between the bonding and AB states of H_2, 9.53 eV, is much larger than the energy of a visible light quantum, no electron in the bonding state of H_2's can be excited by a photon to the AB state to drive the chemical reaction in the visible regime. However, in the coupled system, the AB state is only 1.48 eV above the Fermi level, which suggests the possibility of transferring hot electrons generated in the metallic NP to the AB state of H_2 and inducing chemical reaction such as H_2 dissociation. In addition, Figure 1b also shows that the AB WF of H_2 is strongly hybridized with the NP, which can also facilitate interfacial hot-electron transfer by directly exciting an electron of the NP to the attached molecule, as demonstrated in recent experiments.[44−46] Because

DOI: 10.1021/acsnano.8b03830
ACS Nano XXXX, XXX, XXX−XXX

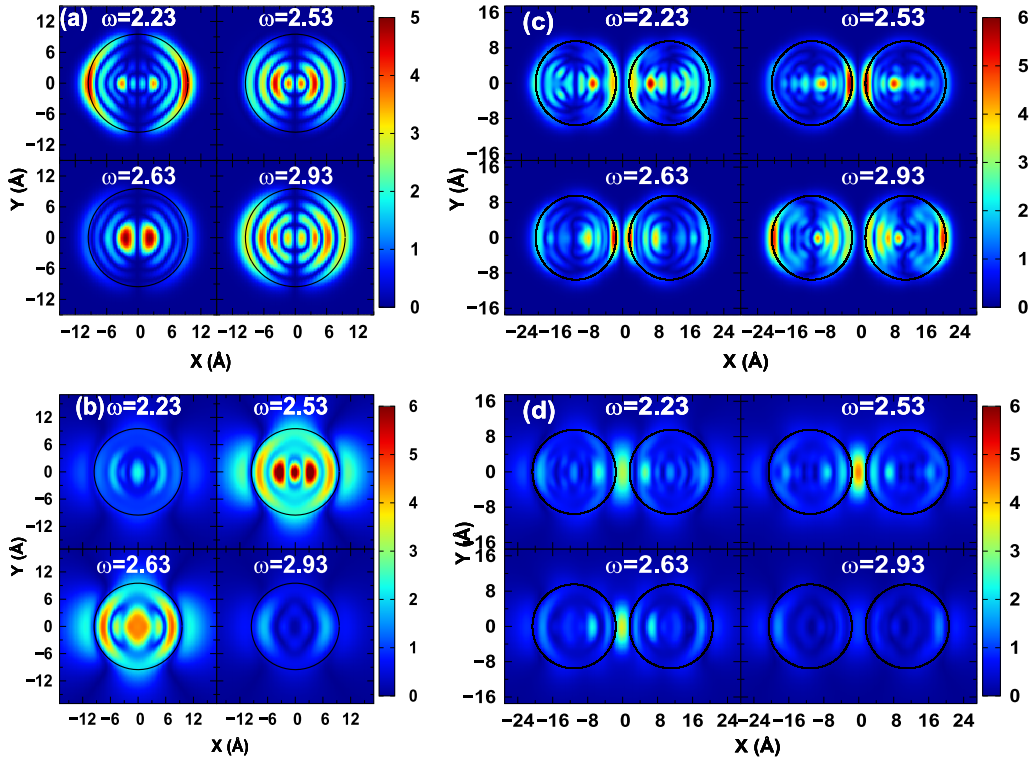

Figure 2. Induced charge (in unit of 10^{-4} e) distribution for a (a) single NP and (c) NP dimer (d = 1.59 Å). Profile of field-enhancement ($\frac{|E_{induced}(\omega)|}{|E_{incident}(\omega)|}$) for a (b) single NP and (d) NP dimer. The single NP enhances the field at both ends of the NP in the direction of the external field. The NP dimer can generate hot-spots in the gap, and the field enhancement in the dimer gap is also found to be larger than that near the surface of the single NP (except for 2.93 eV).

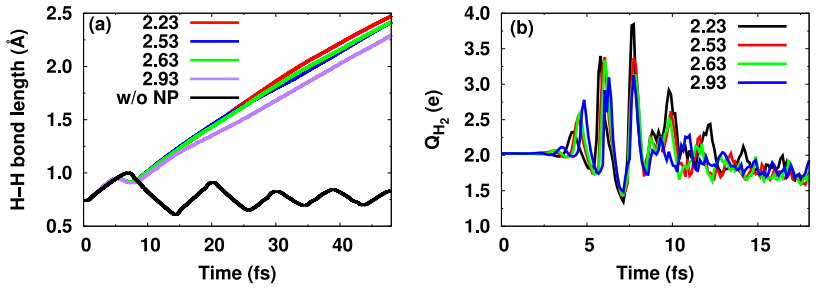

Figure 3. (a) Real-time dynamics of H_2 bond length with and without NP. For the case of H_2 alone, the excitation frequency is 2.53 eV. By coupling to the NP, plasmonic hot-carrier mediated induced chemical reaction is observed. (b) Time evolution of charge around H_2 after photoexcitation with different frequencies.

the excitation of electron−hole pairs by plasmon decay in the NP can generate hot electrons with energy ranging from zero to the photon energy (which means that the energy of hot-electron can be larger than 1.48 eV),[21,47,48] our results suggest that H_2 dissociation can be readily induced by the hot electrons generated in the metallic NP. In addition, the local density of states (LDOS) of H_2 for different H−H bond lengths is plotted in Figure 1d. The evolution of peaks in LDOS for different H−H bond lengths roughly reflects the potential energy surface (PES) of the H_2. The plot shows the evolution of bonding and AB states of H_2 with varying bond length. Even though the H_2 molecule is coupled to the NP and the WFs are hybridized, the PES of H_2 is similar to that of the standalone H_2 molecule. NAMD for the standalone H_2 molecule also confirms that dissociation can indeed occur upon promoting electrons to the antibonding state, as shown in Figure S1. Hence, the PES shown in the plot reveals that even though the H_2 is attached to NP, electron transfer from NP to the AB state of H_2 can indeed drive H_2 dissociation by following the molecular dynamics on the excited state PES.

The absorption spectra of NP and NP + H_2 are shown by Figure 1e. The spectrum of the NP shows four resonant absorption peaks that are all plasmonic, as confirmed by the Casida calculation, in which collective excitations are observed. These four peaks correspond to different plasmon modes[49] (and here, we note that interband effects are not included in the Jellium model, so the optical properties of Au in this model are more plasmonic than they would in a more-realistic description of Au). The distribution of induced charge and field enhancement for each mode can be found in Figure 2a,b. When H_2 is absorbed on the NP surface, the absorption spectrum is weakly perturbed (slightly larger broadening, i.e., damping, to the peaks is observed) because the WF hybridization between the H_2 and the NP alters the electronic

DOI: 10.1021/acsnano.8b03830
ACS Nano XXXX, XXX, XXX−XXX

structure as well as the collective electron oscillation (plasmon) to some extent. However, the four resonant peaks are almost unchanged. The absorption spectrum in the visible is dominated by the NP even though the AB state of H_2 is hybridized with the NP. Because the NP shows stronger absorption and field enhancement at the resonant frequencies, we study next the dynamics of these states, namely, four resonant energies (ω = 2.23, 2.53, 2.63, and 2.93 eV) of the NP are used throughout the manuscript unless specified otherwise to excite the NP and to calculate the subsequent plasmonic hot-carrier-mediated chemical reaction.

Figure 3a plots the time evolution of H−H bond length (with and without NP) excited by the external field with different excitation energies. The black curve shows that the H_2 bond oscillates with the external field and never dissociates if the H_2 is not coupled to NP. Because the energy of incident light is much smaller than the HOMO−LUMO gap, an external field can only perturb the charge density and drive the hydrogen molecule to vibrate near the equilibrium position. However, if the H_2 is placed near the NP surface, plasmon excitation at any resonant energy results in an increase in the H_2 bond length. The H−H bond reaches 2 Å in less than 40 fs, indicating molecular dissociation. Because the Jellium model with no explicit Au atoms is used in our work, the Au−H interaction is not correctly captured, i.e., the adsorption and desorption behavior of H atoms on the NP surface is poorly described. Consequently, the H atoms drift away after dissociation.

To illustrate the charge-transfer behavior, we also analyzed the charge dynamics upon laser excitation. Figure 3b shows the charge around H_2, which is calculated by integrating the charge density within 3 Å of the H_2 molecule. Following the oscillations of the external field, the H_2 charge also oscillates with time, which indicates forward and backward charge transfer between the NP and H_2 molecule. Initially, the Q_{H_2} is around 2 e (elemental charge). After photoexcitation, The charge of H_2 increases to 3.1−3.8 e at around 7.7 fs. The additional charge transferred from the NP resides on the AB states of H_2, driving motion along the excited potential energy surface and dissociating the molecule. Figure 3b shows that the amount of charge transferred to H_2 varies for different excitation energies. Consequently, different excitation energies can result in slightly different dissociation rates because the distribution of induced charge density and field enhancement for different plasmon modes are different as shown in Figure 2a,b. If the excitation energy tunes away from the plasmon resonant energies, the field-enhancement and induced charges become smaller. Consequently, the dissociation rates reduce, as shown in Figure S2. In addition, the charge transfer is also dependent on light intensity. Generally, increasing the light intensity increases the amount of charge transferred to H_2 because the intensity of hot-carriers generated from the plasmon decay is proportional to light intensity in the linear response regime.

Tunable H_2 Dissociation in the Plasmonic Dimer. In practical applications, an assembly of NPs instead of a single NP is usually employed, allowing for the formation of dimers and other aggregates that have more significant electromagnetic hot spots and charge-transfer plasmons.[50] Indeed, plasmonic NP aggregates and arrays have many novel optical properties and have found promising applications in various fields, including lasing, sensing, and quantum information processing.[51] As shown in Figure 2, the distribution of induced charge and field enhancement in the plasmonic dimer is very different from that of a NP monomer. In contrast to a single NP, the field enhancement of the plasmonic dimer is located in the gap and is more significant than that in the near-field of a NP monomer. Because photodissociation also depends on light intensity, as evidenced by Figure S3, the stronger field in the gap then may lead to improved dissociation. Indeed, the field enhancement provided by plasmonic structures has been widely used to enhance chemical reactions.[18] Moreover, as we discussed above, the stronger field intensity is also able to induce more hot electrons, an effect confirmed theoretically and experimentally.[52,53] Thus, it is natural to consider if the stronger field enhancement can facilitate H_2 dissociation. Consequently, we calculated H_2 dissociation in the plasmonic dimer for different geometrical configurations.

As an example of the photochemistry for the dimer structure, we consider the H_2 molecule placed between the NPs. The distance between H_2 and one of the NPs is fixed at 1.59 Å (which we define as the distance D), which is the same as in the case studied above. The distance between H_2 and the other NP is d, taken as a variable. A schematic diagram of the configuration is shown in Figure 4a. The time evolution of H−H bond lengths for different d is plotted in Figure 4b−e. When $d = D$ = 1.59 Å, the H_2 is placed precisely in the center of the plasmonic dimer, with the stronger field enhancement compared to larger values of d, as shown in Figure S4. It should be noted that there is a critical distance between the two NPs at which the field-enhancement is strongest for a general plasmonic dimer.[54] In our case, the smallest separation between the two NPs is 3.18 Å for $d = D$, and the field

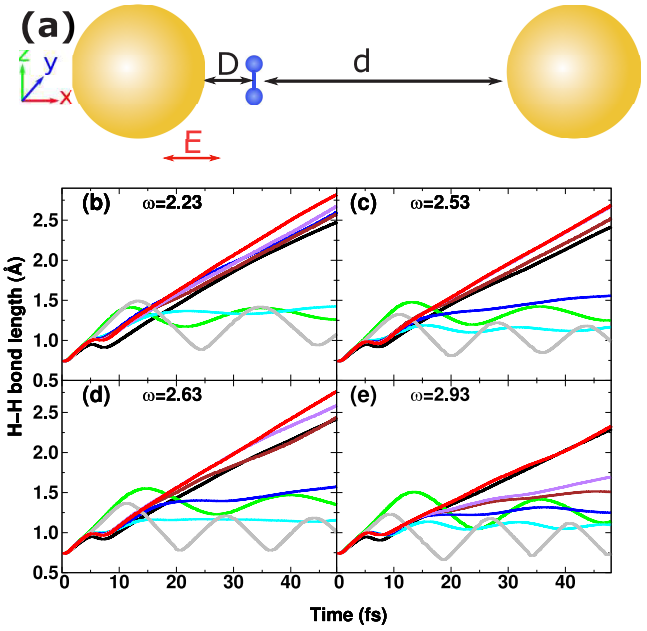

Figure 4. Bond dynamics of H_2 in plasmonic dimer with different distance. H_2 dissociation in a dimer of a pair of 1.9 nm NP with different distances (for D = 1.59 Å): monomer (black), d = 1.59 Å (green), d = 3.70 Å (cyan), d = 5.82 Å (blue), d = 7.94 Å (brown), d = 10.05 Å (purple), d = 12.17 Å (red), and $D = d$ = 5.82 Å (gray). Photochemical reaction for d = 1.59 Å is significantly suppressed. Tuning the distance d can affect the dynamics of H_2 in the plasmonic dimer.

DOI: 10.1021/acsnano.8b03830
ACS Nano XXXX, XXX, XXX−XXX

enhancement decreases monotonically with increasing d. In this configuration, the induced charges (hot electrons) are enhanced in the gap edges (Figure 2c) except for 2.93 eV. The latter is an example of plasmonic resonance in which the induced charges are not enhanced at the gap edges. However, no matter what the excitation energy is, the H−H bond never breaks, as shown by the green curves in Figure 4. Even though Figure 4 suggests that, for geometries with smaller d, the H−H bond length can significantly increases to 1.2−1.4 Å, which is larger than the equilibrium value, the dissociation event does not occur given the subsequent oscillatory dynamics of the bond length.

Our NAMD simulations further demonstrate that tuning the distance d can affect the dynamics significantly. As shown in Figure 4, the H_2 starts to dissociate for some excitation frequencies when d reaches 5.82 Å. It should be noted that d = 5.82 Å may be not a precise critical distance that separates the two phases (H_2 dissociation or lack of dissociation) because we did not sample the distance d with sufficiently small increments due to the computational cost. However, for a given light intensity and photon energy, a critical distance that separates the two phases exists. This critical distance can vary with excitation energy (or plasmon mode) because different plasmon modes induce different charge distributions, field enhancements, and dissociation rates, as shown in Figures 2a,b, and 3a. For instance, for the mode at 2.93 eV, which has a smaller dissociation rate as shown in Figure 3a, larger d is required to restore the chemical reaction, as seen in Figure 4e. To illustrate the importance of the relative position of the H_2 molecule in the plasmonic dimer, we studied the H_2 dynamics in the gap with $D = d$ = 5.82 Å. Here, the distance between the two NPs is 11.64 Å, which is the same as for the arrangement with D = 1.59 Å and d = 10.05 Å. As shown by the gray line in Figure 4, no dissociation is observed in this case, which, however, is similar to outcome with geometry $D = d$ = 1.59 Å. The difference is that when $D = d$ = 5.82 Å, the bond-fluctuation time scale is faster. Moreover, the distance between the H_2 and the NP (5.82 Å) is much larger than 1.59 Å, so the coupling between the H_2 and the NP is much smaller compared to that for the $D = d$ = 1.59 Å geometry, and the H_2 dynamics are closer to those of the pure H_2 case, as shown by the black curve of Figure 3a. An even-larger distance d more strongly favors dissociation of the H−H bond. These results demonstrate that chemical reaction can either be suppressed or enhanced by the plasmonic dimer depending on the relative position of the molecule between the dimer. Thus, hot-carrier-mediated dissociation can be tuned by controlling the location of the molecule in the gap. For the NP dimer, the optical properties are also different from that of a single NP, especially for small d. As shown in Figure S5, compared to a single NP, the resonant peaks are shifted in a dimer with the shift increasing with decreasing d. Some peaks are blue-shifted, and the others are red-shifted because coupling (Δ) between the two NPs can split a resonant energy (ω) into $\omega \pm \Delta$ components. This suggests modeling the H_2 dynamics in the NP dimer for d = 1.59 Å with the new resonant energies (2.16, 2.32, 2.40, and 2.63 eV). The results are shown in Figure S6, and they indicate the absence of H_2 dissociation, even when the H_2 is excited at the resonant energies of the NP dimer.

We have further examined the charge dynamics of the H_2 molecule in the dimer when excited by different photon energies. The results are plotted in Figure 5, and then the charge difference between the two nanoparticles as well as the

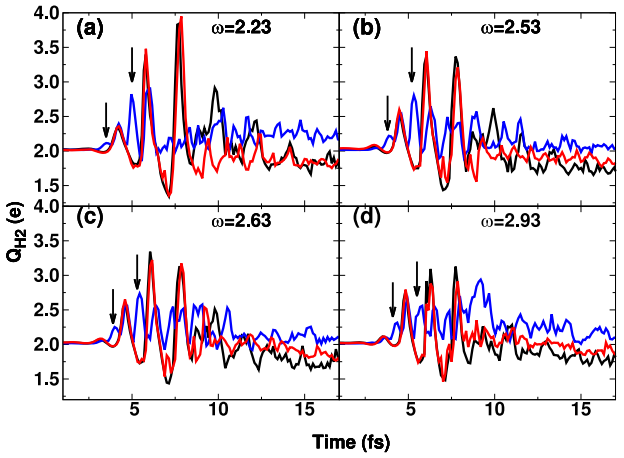

Figure 5. Charge of H_2 on the surface of single NP (black) and in plasmonic dimer with different d: d = 1.59 Å (blue) and d = 12.17 Å (red). In general, the larger distance increases the charge accumulation on the H_2 molecule. For d = 1.59 Å, the hot electrons transferred from the left NP quickly transfer to the right NP, which reduces charge accumulation on H_2. Thus, the photochemical reaction is suppressed.

charges of each NP are plotted in Figure S7. When d = 1.59 Å, the charge dynamics on the H_2 molecule shows high-frequency oscillations (by a factor of 2) but with reduced amplitudes compared to the monomer. In addition, Figure S7 shows that the charge oscillates back and forth between the two nanoparticles with a frequency that is comparable to that seen for the monomer. What these two figures show is that when the nanoparticles are close together and the molecule is midway between them, the charge evolves coherently from one particle to the molecule and to the other particle and then back,, with the doubled frequency at the position of the molecule reflecting a small difference in phasing of the charge flow to the molecule and then from the molecule to the receiving particle. Also note that the charge changes from −4 to +4 for the particles in Figure S7, while the corresponding change on the H_2 is less than 0.5 in magnitude. Hence, compared to the single-NP case (the black curve in Figure 5), the charge accumulation on H_2 is reduced, and dissociation is much less probable. When d = 12.17 Å, the charge oscillation becomes the same as the single NP case, which indicates that this value of d is sufficient to suppress the second charge transfer. The maximum charge on H_2 can reach as high as 3.8 e in this case, which significantly increases the dissociation probability.

Overall, we see that hot carriers transferred from one NP to the H_2 will undergo another charge transfer to the other NP before H_2 dissociation can develop when d = 1.59 Å. Increasing the distance d makes the charge-transfer rates different. Indeed, in the red curves in Figure 5, we see that the time scale of charge oscillation is the same as the single-NP case. With increasing distance, the charge loss from the H_2 molecule to the right NP is suppressed. At a certain distance, the charge accumulation on H_2 can be large enough to induce bond dissociation. This is the reason why a critical distance exists for inducing H_2 dissociation in the plasmonic dimer. Note that the right NP still has a significant contribution to the field enhancement in the gap for d = 12.17 Å (see Figure S8), so dissociation can be enhanced relative to the monomer case for certain d values and plasmon modes.

DOI: 10.1021/acsnano.8b03830
ACS Nano XXXX, XXX, XXX−XXX

DISCUSSION

In realistic applications, the H_2 molecule would typically have a broad spatial distribution of possible locations on the dimer, and it is not possible to control this with any precision. Hence, only a fraction of the H_2 molecules in a strong plasmonic field can be dissociated by exciting plasmonic hot carriers. To improve efficiency, charge transfer from the H_2 molecule to one of the NPs needs to be suppressed. One approach is to coat one of the particles with SiO_2. Recent experiments have indicated that the large barrier between SiO_2 and a metallic NP can significantly prevent hot electron transfer.[55] In addition, it should be noted that plasmon-driven hot-electron transfer to adsorbed molecules (in this case, the molecule 4,4′-bipyridine, BPY that has a stable negative ion) has been confirmed in a recent experiment using surface-enhanced Raman scattering techniques (SERS).[56] This study also found that the negative ion has a finite lifetime, indicating that additional charge-transfer processes occur after the negative ion is formed. Unfortunately, the time scale of charge-transfer processes could only be studied at time scales greater than 1 s in that work. In addition, the quantum yield (QY) of H_2 dissociation is not studied in this work. In principle, the generated hot electron will lose energy *via* electron−electron and electron−phonon interactions as well as system−bath coupling. In the Jellium model, there are no nuclear vibrational effects, but because the system is coupled to a thermal bath, the additional energy will dissipate to the bath. The QY can be estimated from evolution of trajectory ensemble during molecular dynamics starting with different initial excited states. However, we did not conduct such simulations in the Octopus software due to the numerical cost and approximate nature of the results.

Finally, we note that the mechanism of suppression of chemical reaction in the plasmonic dimer proposed in this work is fundamentally different from that studied in ref 57, where the quantum nature of the cavity plays a vital role in modifying the PES of the molecule.[58,59] In contrast, in our case, the balance between charge transfer and field enhancement tunes the chemical reaction, and strong coupling leading to the formation of a new polaritonic state is not needed. Another aspect of the difference in the mechanisms is that the suppression of chemical reaction when d = 1.59 Å holds for different excitation frequencies, including nonresonant. The mechanism in ref 57 only holds for resonant excitation because hybridization between the electronic and photonic states is only important when the excitation energy is resonant with the gap.[58]

CONCLUSIONS

In summary, we have performed TDDFT and NAMD calculations, which enable us to directly look at the dynamic process of H_2 dissociation on the surface of a metallic NP. Our results illustrate the mechanism of plasmon-induced H_2 dissociation at the atomic scale and identify how hot carriers can be transferred from a NP to the adsorbed molecule to drive photochemistry. The electronic structure calculations show significant wave function hybridization between NP and H_2 and that the energy difference between the AB state and the Fermi level makes dissociation accessible by the visible light. In addition, because photoinduced charge transfer can be controlled by the shape of the external field, we can imagine adjusting laser parameters and nanoparticle size to control electronic hybridization and dynamics to improve the plasmon-assisted photochemistry.

Our results also demonstrate that the photochemistry can be tunable in the case of a plasmonic dimer. When the molecule is placed in the center of NP dimer, charge transfer between the molecule and each of the two NPs is identical. Consequently, the hot electrons transferred to the molecule from one of the NP are transferred to the other nanoparticle before the dissociation can occur. As a result, the effective charge accumulation on the molecule is reduced, and the chemical reaction is suppressed. By the tuning of the relative position of the molecule in the gap of the NP dimer, one of the charge-transfer processes can be efficiently suppressed. Consequently, charge accumulation on the molecule can be enhanced and the chemical reactions restored. This indicates that by carefully tuning geometry, field enhancement can be increased and charge loss minimized. Even though, our conclusions are based on H_2 dissociation, the concept can be applied to other cases, such as water splitting (results not shown). In practical applications, the loss of charge from an adsorbate to the NP can be suppressed *via* coating of the latter by insulating materials, such as SiO_2.

METHODS

The calculations are carried out using the real-space time-dependent density functional theory (TDDFT) code OCTOPUS (version 7.1).[40−42] The nanoparticle is approximated as Jellium medium with a single electron radius (Wigner-Seitz radius)[42] of r_s = 4.5 au. The radius is carefully chosen so that the resonant frequencies of the NP are similar to that of Au nanoparticles with a diameter of several nanometers. The diameter of the NP is 38 au., i.e., 64 free electrons in the NP. Localized density approximation (LDA) is employed in the calculation. The choice of LDA functional in this work underestimates the HOMO−LUMO gap of H_2. However, this does not affect the physics and conclusions covered in this work. Using other functionals, such as PBE, gives similar results. The grid in real space is set as 0.5 au. Nonadiabatic molecular dynamics is treated within the Ehrenfest scheme with temperature fluctuation around the room temperature (300 K). The ground state is used as the initial state for NAMD simulations. Time step of 0.1 au is used in the calculation. For the optical absorption spectrum, a electrical pulse (δ function) is used.

The external electric field of the light is set to $E(t) = E_{max}\exp\left[-\frac{(t-t_0)^2}{2\tau^2}\right]\cos[\omega(t-t_0)]$, where ω is the excitation frequency. E_{max} is the maximum field strength of the laser pulse. τ = 1.6 fs is the width of the pulse, and t_0 = 6.6 fs is the center of the pulse. Figure S3 indicates that a critical laser intensity is required to observe H_2 dissociation within 100 fs, and similar phenomena was also observed in a recent experiment.[25] In addition, it should be noted that the laser intensity used in this work is much higher than that in experiment due to the following: (1) we need to observe the H_2 dissociation in tens of femtoseconds due to the computational cost; (2) even though the laser field seems very strong, the pulse duration is very short (∼10 fs) compared to the illumination time (∼1 s) used in the experiment, and as a result, the energy provided to the system is comparable to one photon; and (3) the plasmon enhancement in our model is expected to be smaller than that in the experiment because the experiment involves larger particles and aggregates that have more significant electromagnetic hot spots.

The contribution (weight) of H_2 to each WF is estimated by integrating the WFs in a sphere centered at each H atom with a radius of 3 Å, i.e., $w_i = \int_{r\le 3 \text{ and } r\notin NP} \phi_i(\mathbf{r})\phi_i^*(\mathbf{r})d\mathbf{r}$. It should also be noted that the choice of radius does not affect our conclusion. If a smaller radius is used to estimate the WF weight, a similar result (LDOS of H_2 for different bond lengths) can also be obtained (with the only difference being that the WF weights become smaller). The charge around the H_2 is calculated by integrating the charge density within 3

DOI: 10.1021/acsnano.8b03830
ACS Nano XXXX, XXX, XXX−XXX

Å of the H_2 molecule, $Q_{H_2}(t) = \int_{|r-r_{H_2}|\leq 3 \text{ and } r\notin NP} \rho(\mathbf{r}, t)d\mathbf{r}$. According to our test, 3 Å is a reasonable threshold with which to define the H_2 density. A radius larger than 3 Å (recall that the position in the Jellium approximation is excluded in the integration) does not increase the charge number on H_2. Similarly, the charge on Au is calculated by integrating charge density within 15 Å (excluding the volume used to calculate the H_2 charge). This radius (15 Å) used to calculate the Au charge is larger than the NP radius (9.525 Å) because the charge density will extend outside the sphere, as shown by Figure 2a. This evidence that the majority of the charge is localized in Au, as can be seen by examining the respective density distribution. In addition, the dissociation rate is defined as the inverse of time required for splitting the H−H bond when the length reaches 2.0 Å.

In addition, it should be noted that a single trajectory is used in the simulations presented in main text to reduce computational cost. However, the results also hold for many-trajectories, as shown in Figure S9, where statistical results for 20 trajectories for a certain frequency (2.53 eV) are given for the single NP case and the NP dimer and with d being 1.59 and 12.17 Å. For the single-trajectory simulation presented in the main text, the initial velocities of the ions are set to zero. For the many-trajectories simulations shown in the Supporting Information, the bond length and initial velocities are set randomly.

ASSOCIATED CONTENT

Supporting Information

The Supporting Information is available free of charge on the ACS Publications website at DOI: 10.1021/acsnano.8b03830.

Figures showing the dnamics of H_2 bond length without NP, H_2 dissociation rates, field enhancement at the center of the NP dimer, absorption spectra, bond dynamics of H_2, the time evolution of charges on NPs and charge difference between the two NPs, field enhancements of dimer with d = 12.17 Å, and an assembly of NAMD trajectories for the single NP and the NP dimer with d being 1.59 and 12.17 Å. (PDF)

AUTHOR INFORMATION

Corresponding Author

*E-mail: zhy@lanl.gov.

ORCID

Yu Zhang: 0000-0001-8938-1927

Tammie Nelson: 0000-0002-3173-5291

Sergei Tretiak: 0000-0001-5547-3647

Hua Guo: 0000-0001-9901-053X

George C. Schatz: 0000-0001-5837-4740

Notes

The authors declare no competing financial interest.

ACKNOWLEDGMENTS

The work at Northwestern University was supported by the Department of Energy, Office of Basic Energy Sciences, under grant no. DE-FG02-10ER16153 (Y.Z. and G.C.S.). H.G. thanks the support from the Air Force Office of Scientific Research under grant no. FA9550-15-1-0305. The work at Los Alamos National Laboratory (LANL) was supported by the LANL Directed Research and Development Funds (LDRD) (Y.Z., S.T., and T.N.) and performed in part at the Center for Integrated Nanotechnologies (CINT), a U.S. Department of Energy Office of Science user facility at LANL. This research used resources provided by the LANL Institutional Computing (IC) Program. LANL is operated by Los Alamos National Security, LLC, for the National Nuclear Security Administration of the U.S. Department of Energy under contract no. DE-AC52-06NA25396.

REFERENCES

(1) Tame, M. S.; McEnery, K. R.; Ozdemir, S. K.; Lee, J.; Maier, S. A.; Kim, M. S. Quantum Plasmonics. *Nat. Phys.* **2013**, *9*, 329−340.

(2) Archambault, A.; Marquier, F.; Greffet, J.-J.; Arnold, C. Quantum Theory of Spontaneous and Stimulated Emission of Surface Plasmons. *Phys. Rev. B: Condens. Matter Mater. Phys.* **2010**, *82*, 035411.

(3) Ballester, D.; Tame, M. S.; Lee, C.; Lee, J.; Kim, M. S. Long-Range Surface-Plasmon-Polariton Excitation at The Quantum Level. *Phys. Rev. A: At., Mol., Opt. Phys.* **2009**, *79*, 053845.

(4) Kottmann, J. P.; Martin, O. J. F.; Smith, D. R.; Schultz, S. Plasmon Resonances of Silver Nanowires with a Nonregular Cross Section. *Phys. Rev. B: Condens. Matter Mater. Phys.* **2001**, *64*, 235402.

(5) Kelly, K. L.; Coronado, E.; Zhao, L. L.; Schatz, G. C. The Optical Properties of Metal Nanoparticles: The Influence of Size, Shape, and Dielectric Environment. *J. Phys. Chem. B* **2003**, *107*, 668−677.

(6) Brongersma, M. L.; Halas, N. J.; Nordlander, P. Plasmon-Induced Hot Carrier Science and Technology. *Nat. Nanotechnol.* **2015**, *10*, 25−34.

(7) West, P.; Ishii, S.; Naik, G.; Emani, N.; Shalaev, V.; Boltasseva, A. Searching for Better Plasmonic Materials. *Laser Photonics Rev.* **2010**, *4*, 795−808.

(8) Tisdale, W. A.; Williams, K. J.; Timp, B. A.; Norris, D. J.; Aydil, E. S.; Zhu, X.-Y. Hot-Electron Transfer from Semiconductor Nanocrystals. *Science* **2010**, *328*, 1543−1547.

(9) Wang, F.; Melosh, N. A. Plasmonic Energy Collection through Hot Carrier Extraction. *Nano Lett.* **2011**, *11*, 5426−5430.

(10) Clavero, C. Plasmon-Induced Hot-Electron Generation at Nanoparticle/Metal-Oxide Interfaces for Photovoltaic and Photocatalytic Devices. *Nat. Photonics* **2014**, *8*, 95−103.

(11) Dong, Y.; Choi, J.; Jeong, H.-K.; Son, D. H. Hot Electrons Generated from Doped Quantum Dots *via* Upconversion of Excitons to Hot Charge Carriers for Enhanced Photocatalysis. *J. Am. Chem. Soc.* **2015**, *137*, 5549−5554.

(12) Baffou, G.; Quidant, R. Nanoplasmonics for Chemistry. *Chem. Soc. Rev.* **2014**, *43*, 3898−3907.

(13) Boriskina, S. V.; Ghasemi, H.; Chen, G. Plasmonic Materials for Energy: From Physics to Applications. *Mater. Today* **2013**, *16*, 375−386.

(14) Fang, Z.; Wang, Y.; Liu, Z.; Schlather, A.; Ajayan, P. M.; Koppens, F. H. L.; Nordlander, P.; Halas, N. J. Plasmon-Induced Doping of Graphene. *ACS Nano* **2012**, *6*, 10222−10228.

(15) Hong, T.; Chamlagain, B.; Hu, S.; Weiss, S. M.; Zhou, Z.; Xu, Y.-Q. Plasmonic Hot Electron Induced Photocurrent Response at MoS_2-Metal Junctions. *ACS Nano* **2015**, *9*, 5357−5363.

(16) Reineck, P.; Brick, D.; Mulvaney, P.; Bach, U. Plasmonic Hot Electron Solar Cells: The Effect of Nanoparticle Size on Quantum Efficiency. *J. Phys. Chem. Lett.* **2016**, *7*, 4137−4141.

(17) Knight, M. W.; Sobhani, H.; Nordlander, P.; Halas, N. J. Photodetection with Active Optical Antennas. *Science* **2011**, *332*, 702−704.

(18) Zhang, Y.; He, S.; Guo, W.; Hu, Y.; Huang, J.; Mulcahy, J. R.; Wei, W. D. Surface-Plasmon-Driven Hot Electron Photochemistry. *Chem. Rev.* **2018**, *118*, 2927−2954.

(19) Naik, G. V.; Dionne, J. A. Photon Upconversion with Hot Carriers in Plasmonic Systems. *Appl. Phys. Lett.* **2015**, *107*, 133902.

(20) Kojori, H. S.; Yun, J.-H.; Paik, Y.; Kim, J.; Anderson, W. A.; Kim, S. J. Plasmon Field Effect Transistor for Plasmon to Electric Conversion and Amplification. *Nano Lett.* **2016**, *16*, 250−254.

(21) Zhang, Y.; Yam, C.; Schatz, G. C. Fundamental Limitations to Plasmonic Hot-Carrier Solar Cells. *J. Phys. Chem. Lett.* **2016**, *7*, 1852−1858.

(22) Palczewski, K. Chemistry and Biology of Vision. *J. Biol. Chem.* **2012**, *287*, 1612−1619.

DOI: 10.1021/acsnano.8b03830
ACS Nano XXXX, XXX, XXX−XXX

(23) Blankenship, R. *Molecular Mechanisms of Photosynthesis*; John Wiley & Sons: Hoboken, NJ, 2014.
(24) Zemelman, B. V.; Nesnas, N.; Lee, G. A.; Miesenböck, G. Photochemical Gating of Heterologous Ion Channels: Remote Control over Genetically Designated Populations of Neurons. *Proc. Natl. Acad. Sci. U. S. A.* **2003**, *100*, 1352−1357.
(25) Mukherjee, S.; Libisch, F.; Large, N.; Neumann, O.; Brown, L. V.; Cheng, J.; Lassiter, J. B.; Carter, E. A.; Nordlander, P.; Halas, N. J. Hot Electrons Do the Impossible: Plasmon-Induced Dissociation of H_2 on Au. *Nano Lett.* **2013**, *13*, 240−247.
(26) Libisch, F.; Cheng, J.; Carter, E. A. Electron-Transfer-Induced Dissociation of H_2 on Gold Nanoparticles: Excited-State Potential Energy Surfaces *via* Embedded Correlated Wavefunction Theory. *Z. Phys. Chem.* **2013**, *227*, 1455−1466.
(27) Linic, S.; Aslam, U.; Boerigter, C.; Morabito, M. Photochemical Transformations on Plasmonic Metal Nanoparticles. *Nat. Mater.* **2015**, *14*, 567.
(28) Christopher, P.; Xin, H.; Marimuthu, A.; Linic, S. Singular Characteristics and Unique Chemical Bond Activation Mechanisms of Photocatalytic Reactions on Plasmonic Nanostructures. *Nat. Mater.* **2012**, *11*, 1044.
(29) Mukherjee, S.; Zhou, L.; Goodman, A. M.; Large, N.; Ayala-Orozco, C.; Zhang, Y.; Nordlander, P.; Halas, N. J. Hot-Electron-Induced Dissociation of H_2 on Gold Nanoparticles Supported on SiO_2. *J. Am. Chem. Soc.* **2014**, *136*, 64−67.
(30) Zhang, C.; Zhao, H.; Zhou, L.; Schlather, A. E.; Dong, L.; McClain, M. J.; Swearer, D. F.; Nordlander, P.; Halas, N. J. Al-Pd Nanodisk Heterodimers as Antenna-Reactor Photocatalysts. *Nano Lett.* **2016**, *16*, 6677−6682.
(31) Swearer, D. F.; Zhao, H.; Zhou, L.; Zhang, C.; Robatjazi, H.; Martirez, J. M. P.; Krauter, C. M.; Yazdi, S.; McClain, M. J.; Ringe, E.; Carter, E. A.; Nordlander, P.; Halas, N. J. Heterometallic Antenna-Reactor Complexes for Photocatalysis. *Proc. Natl. Acad. Sci. U. S. A.* **2016**, *113*, 8916−8920.
(32) Yan, L.; Ding, Z.; Song, P.; Wang, F.; Meng, S. Plasmon-Induced Dynamics of H_2 Splitting on a Silver Atomic Chain. *Appl. Phys. Lett.* **2015**, *107*, 083102.
(33) Ingram, D. B.; Linic, S. Water Splitting on Composite Plasmonic-Metal/Semiconductor Photoelectrodes: Evidence for Selective Plasmon-Induced Formation of Charge Carriers near the Semiconductor Surface. *J. Am. Chem. Soc.* **2011**, *133*, 5202−5205.
(34) Ghobadi, T. G. U.; Ghobadi, A.; Ozbay, E.; Karadas, F. Strategies for Plasmonic Hot-Electron-Driven Photoelectrochemical Water Splitting. *ChemPhotoChem.* **2018**, *2*, 161−182.
(35) Naldoni, A.; Guler, U.; Wang, Z.; Marelli, M.; Malara, F.; Meng, X.; Besteiro, L. V.; Govorov, A. O.; Kildishev, A. V.; Boltasseva, A.; Shalaev, V. M. Broadband Hot-Electron Collection for Solar Water Splitting with Plasmonic Titanium Nitride. *Adv. Opt. Mater.* **2017**, *5*, 1601031.
(36) Lee, J.; Mubeen, S.; Ji, X.; Stucky, G. D.; Moskovits, M. Plasmonic Photoanodes for Solar Water Splitting with Visible Light. *Nano Lett.* **2012**, *12*, 5014−5019.
(37) Robatjazi, H.; Bahauddin, S. M.; Doiron, C.; Thomann, I. Direct Plasmon-Driven Photoelectrocatalysis. *Nano Lett.* **2015**, *15*, 6155−6161.
(38) Mubeen, S.; Lee, J.; Singh, N.; Kramer, S.; Stucky, G. D.; Moskovits, M. An Autonomous Photosynthetic Device in Which All Charge Carriers Derive From Surface Plasmons. *Nat. Nanotechnol.* **2013**, *8*, 247−251.
(39) Hou, W.; Hung, W. H.; Pavaskar, P.; Goeppert, A.; Aykol, M.; Cronin, S. B. Photocatalytic Conversion of CO_2 to Hydrocarbon Fuels *via* Plasmon-Enhanced Absorption and Metallic Interband Transitions. *ACS Catal.* **2011**, *1*, 929−936.
(40) Castro, A.; Appel, H.; Oliveira, M.; Rozzi, C. A.; Andrade, X.; Lorenzen, F.; Marques, M. A. L.; Gross, E. K. U.; Rubio, A. Octopus: a Tool for the Application of Time-Dependent Density Functional Theory. *Phys. Status Solidi B* **2006**, *243*, 2465−2488.
(41) Andrade, X.; Alberdi-Rodriguez, J.; Strubbe, D. A.; Oliveira, M. J. T.; Nogueira, F.; Castro, A.; Muguerza, J.; Arruabarrena, A.; Louie, S. G.; Aspuru-Guzik, A.; Rubio, A.; Marques, M. A. L. Time-Dependent Density-Functional Theory in Massively Parallel Computer Architectures: the Octopus Project. *J. Phys.: Condens. Matter* **2012**, *24*, 233202.
(42) Andrade, X.; Strubbe, D.; De Giovannini, U.; Larsen, A. H.; Oliveira, M. J. T.; Alberdi-Rodriguez, J.; Varas, A.; Theophilou, I.; Helbig, N.; Verstraete, M. J.; Stella, L.; Nogueira, F.; Aspuru-Guzik, A.; Castro, A.; Marques, M. A. L.; Rubio, A. Real-Space Grids and the Octopus Code as Tools for the Development of New Simulation Approaches for Electronic Systems. *Phys. Chem. Chem. Phys.* **2015**, *17*, 31371−31396.
(43) Jensen, L.; Aikens, C. M.; Schatz, G. C. Electronic Structure Methods for Studying Surface-Enhanced Raman Scattering. *Chem. Soc. Rev.* **2008**, *37*, 1061−1073.
(44) Wu, K.; Chen, J.; McBride, J. R.; Lian, T. Efficient Hot-Electron Transfer by a Plasmon-Induced Interfacial Charge-Transfer Transition. *Science* **2015**, *349*, 632−635.
(45) Boerigter, C.; Campana, R.; Morabito, M.; Linic, S. Evidence and Implications of Direct Charge Excitation as the Dominant Mechanism in Plasmon-Mediated Photocatalysis. *Nat. Commun.* **2016**, *7*, 10545.
(46) Boerigter, C.; Aslam, U.; Linic, S. Mechanism of Charge Transfer from Plasmonic Nanostructures to Chemically Attached Materials. *ACS Nano* **2016**, *10*, 6108−6115.
(47) Bernardi, M.; Mustafa, J.; Neaton, J. B.; Louie, S. G. Theory and Computation of Hot Carriers Generated by Surface Plasmon Polaritons in Noble Metals. *Nat. Commun.* **2015**, *6*, 7044.
(48) Sundararaman, R.; Narang, P.; Jermyn, A. S.; Goddard Iii, W. A.; Atwater, H. A. Theoretical Predictions for Hot-Carrier Generation from Surface Plasmon Decay. *Nat. Commun.* **2014**, *5*, 5788.
(49) Townsend, E.; Bryant, G. W. Plasmonic Properties of Metallic Nanoparticles: The Effects of Size Quantization. *Nano Lett.* **2012**, *12*, 429−434.
(50) Zhu, W.; Esteban, R.; Borisov, A. G.; Baumberg, J. J.; Nordlander, P.; Lezec, H. J.; Aizpurua, J.; Crozier, K. B. Quantum Mechanical Effects in Plasmonic Structures with Subnanometre Gaps. *Nat. Commun.* **2016**, *7*, 11495.
(51) Wang, D.; Yang, A.; Wang, W.; Hua, Y.; Schaller, R. D.; Schatz, G. C.; Odom, T. W. Band-Edge Engineering for Controlled Multi-Modal Nanolasing in Plasmonic Superlattices. *Nat. Nanotechnol.* **2017**, *12*, 889−894.
(52) Harutyunyan, H.; Martinson, A. B. F.; Rosenmann, D.; Khorashad, L. K.; Besteiro, L. V.; Govorov, A. O.; Wiederrecht, G. P. Anomalous Ultrafast Dynamics of Hot Plasmonic Electrons in Nanostructures with Hot Spots. *Nat. Nanotechnol.* **2015**, *10*, 770.
(53) Besteiro, L. V.; Govorov, A. O. Amplified Generation of Hot Electrons and Quantum Surface Effects in Nanoparticle Dimers with Plasmonic Hot Spots. *J. Phys. Chem. C* **2016**, *120*, 19329−19339.
(54) Marinica, D.; Kazansky, A.; Nordlander, P.; Aizpurua, J.; Borisov, A. G. Quantum Plasmonics: Nonlinear Effects in the Field Enhancement of a Plasmonic Nanoparticle Dimer. *Nano Lett.* **2012**, *12*, 1333−1339.
(55) Cushing, S. K.; Li, J.; Bright, J.; Yost, B. T.; Zheng, P.; Bristow, A. D.; Wu, N. Controlling Plasmon-Induced Resonance Energy Transfer and Hot Electron Injection Processes in Metal@TiO_2 Core-Shell Nanoparticles. *J. Phys. Chem. C* **2015**, *119*, 16239−16244.
(56) Sprague-Klein, E. A.; McAnally, M. O.; Zhdanov, D. V.; Zrimsek, A. B.; Apkarian, V. A.; Seideman, T.; Schatz, G. C.; Van Duyne, R. P. Observation of Single Molecule Plasmon-Driven Electron Transfer in Isotopically Edited 4,4'-Bipyridine Gold Nanosphere Oligomers. *J. Am. Chem. Soc.* **2017**, *139*, 15212−15221.
(57) Galego, J.; Garcia-Vidal, F. J.; Feist, J. Suppressing Photochemical Reactions with Quantized Light Fields. *Nat. Commun.* **2016**, *7*, 13841.
(58) Hutchison, J. A.; Schwartz, T.; Genet, C.; Devaux, E.; Ebbesen, T. W. Modifying Chemical Landscapes by Coupling to Vacuum Fields. *Angew. Chem., Int. Ed.* **2012**, *51*, 1592−1596.
(59) Feist, J.; Galego, J.; Garcia-Vidal, F. J. Polaritonic Chemistry with Organic Molecules. *ACS Photonics* **2018**, *5*, 205−216.

DOI: 10.1021/acsnano.8b03830
ACS Nano XXXX, XXX, XXX−XXX